remote sensing

MDPI

Article

A Live Fuel Moisture Content Product from Landsat TM Satellite Time Series for Implementation in Fire Behavior Models

Mariano García [1,2], David Riaño [3,4,*], Marta Yebra [5,6,7], Javier Salas [1], Adrián Cardil [8,9], Santiago Monedero [8], Joaquín Ramirez [9], M. Pilar Martín [3], Lara Vilar [3], John Gajardo [10] and Susan Ustin [4]

1 Environmental Remote Sensing Research Group, Department of Geology, Geography and the Environment, Universidad de Alcalá, Calle Colegios 2, 28801 Alcalá de Henares, Spain; mariano.garcia@uah.es (M.G.); javier.salas@uah.es (J.S.)
2 Complutum Tecnologías de la Información Geográfica S.L. (COMPLUTIG), Colegios, 2, 28801 Alcalá de Henares, Spain
3 Environmental Remote Sensing and Spectroscopy Laboratory (SpecLab), Spanish National Research Council (CSIC), 28037 Madrid, Spain; mpilar.martin@cchs.csic.es (M.P.M.); lara.vilar@cchs.csic.es (L.V.)
4 Center for Spatial Technologies and Remote Sensing (CSTARS), John Muir Institute of the Environment, University of California Davis, One Shields Drive, Davis, CA 95616, USA; slustin@ucdavis.edu
5 Fenner School of Environment & Society, Colleges of Science, The Australian National University, Acton, ACT 2601, Australia; marta.yebra@anu.edu.au
6 Bushfire and Natural Hazards Cooperative Research Centre, 340 Albert St., East Melbourne, Victoria 3002, Australia
7 Research School of Aerospace, Mechanical and Environmental Engineering, College of Engineering and Computer Science, The Australian National University, Acton, ACT 2601, Australia
8 Technosylva, 24009 León, Spain; acardil@tecnosylva.com (A.C.); smonedero@tecnosylva.com (S.M.)
9 Technosylva, La Jolla, CA 92037-7231, USA; jramirez@tecnosylva.com
10 Instituto de Bosques y Sociedad, Facultad de Ciencias Forestales Y Recursos Naturales, Universidad Austral de Chile, Campus Isla Teja, Valdivia 5090000, Chile; john.gajardo@uach.cl
* Correspondence: david.riano@cchs.csic.es

Received: 10 April 2020; Accepted: 24 May 2020; Published: 27 May 2020

Abstract: Live Fuel Moisture Content (LFMC) contributes to fire danger and behavior, as it affects fire ignition and propagation. This paper presents a two layered Landsat LFMC product based on topographically corrected relative Spectral Indices (SI) over a 2000–2011 time series, which can be integrated into fire behavior simulation models. Nine chaparral sampling sites across three Landsat -5 Thematic Mapper (TM) scenes were used to validate the product over the Western USA. The relations between field-measured LFMC and Landsat-derived SIs were strong for each individual site but worsened when pooled together. The Enhanced Vegetation Index (EVI) presented the strongest correlations (r) and the least Root Mean Square Error (RMSE), followed by the Normalized Difference Infrared Index (NDII), Normalized Difference Vegetation Index (NDVI) and Visible Atmospherically Resistant Index (VARI). The relations between LFMC and the SIs for all sites improved after using their relative values and relative LFMC, increasing r from 0.44 up to 0.69 for relative EVI (relEVI), the best predictive variable. This relEVI served to estimate the herbaceous and woody LFMC based on minimum and maximum seasonal LFMC values. The understory herbaceous LFMC on the woody pixels was extrapolated from the surrounding pixels where the herbaceous vegetation is the top layer. Running simulations on the Wildfire Analyst (WFA) fire behavior model demonstrated that this LFMC product alone impacts significantly the fire spatial distribution in terms of burned probability, with average burned area differences over 21% after 8 h burning since ignition, compared to commonly carried out simulations based on constant values for each fuel model. The method could be applied to Landsat-7 and -8 and Sentinel-2A and -2B after proper sensor inter-calibration and topographic correction.

Keywords: live fuel moisture content; Landsat-5 TM; fire behavior simulator; fire danger; fire propagation; data normalization

1. Introduction

Fire disturbances play a key role in vegetation succession, as well as in the ecosystem's structure and function [1]. Live and dead biomass constitutes the fuel that burns during a fire, and the fuel properties describe their state or moisture content, as well as their spatial distribution and impact on fire spread, intensity and severity [2]. Among these properties, fire ignition and propagation depend on Live Fuel Moisture Content (LFMC) [3–6]. Fuels with high LFMC take longer to ignite as water acts as a heat sink, slowing down fire spread and intensity [5,7]. LFMC is defined as the amount of water in the fuel over its dry weight times 100. This amount of water is calculated as the difference between the fresh weight and the oven-dried weight at 60–100 °C for 24–48 h [5]. More recently, Matthews [8] suggested to dry samples at 105 °C to ensure complete water removal from the samples. The US National Fire Danger Rating System (NFDRS) distinguishes annual and perennial herbaceous LFMC depending on how the drying of the live fuel occurs throughout the year [9]. In addition, the NFDRS also considers the woody LFMC, measuring the moisture of the foliage and of small twigs that are < 0.6 cm [9].

Climate and plant adaptation strategies to drought play a key role on LFMC, with changes in the water content of leaves as well as in dry matter [10]. LFMC remote sensing estimates rely on the spectral changes due to the direct impact of liquid water absorption features and the indirect impact of pigment and structural changes associated with water content variation [11]. Two different approaches have been applied to monitor LFMC from remote sensing data: empirical Spectral Indices (SI) [12–14] and radiative transfer models (RTM) [15–17]. RTM only outperforms empirical models if they are appropriately parameterized and constrained, which requires accurate structural information [15]. Yebra et al. [11] provide a complete review on these methods and their operational implications.

Fire management tools demand comprehensive spatial and temporal LFMC coverage [18]. Therefore, field sampling only serves to calibrate and validate these remote sensing estimates. Operational LFMC remote sensing products benefit fire behavior models, as they can improve fire growth simulations. Most fire simulators generally include a constant LFMC value for each fuel model, thus missing the spatial LFMC variability across the landscape. The Modeling Dynamic Fuels with an Index System (MoD-FIS) from the LANDFIRE program (https://www.landfire.gov/; last accessed 3 April 2020) goes further, detecting the key seasonal changes in herbaceous vegetation to adjust their dynamic fuel models. However, operational tools such as Wildfire Analyst (WFA, http://wildfireanalyst.com/ [19]) demands operational spatially and temporally explicit LFMC products to better estimate fire behavior. Based on BEHAVE surface fire behavior model [2], WFA already digests current spatial weather data available in real time and allows the inclusion of predefined LFMC layers as an input. Other software like FlamMap (https://www.firelab.org/project/flammap/; last accessed 3 April 2020) or FARSITE (https://www.firelab.org/project/farsite/; last accessed April 3rd, 2020) do not include LFMC as a layer.

A common limitation in fire behavior models is also that they require herbaceous and woody LFMC, whereas optical remote sensing is only sensitive to the top layer. An alternative is to use meteorological phenological models like the Growing Season Index (GSI) [20]. The 2016 NFDRS depends on this index to predict herbaceous and woody LFMC. Despite this, the index requires extrapolation from meteorological locations to build a spatially comprehensive LFMC map.

High temporal resolution sensors such as AVHRR [13,21] or MODIS [16,22] or VIIRS, allow the capturing of daily changes in LFMC. Nevertheless, cloud coverage can reduce their effective temporal resolution. Besides, spatial heterogeneity of fuels limits their application, due to their low spatial resolution ($\geq$ 250 m). Medium spatial resolution (20–30 m) sensors, such as Landsat-5 Thematic

Mapper (TM), enable a better spatial characterization [23], but only once every 16 days until its decommission. The combination of Landsat-7 and 8, and Sentinel-2A and 2B ensures an overpass every 3 days at the equator and nearly daily at mid-latitudes at 10–30 m spatial resolution [24]. After proper sensor inter-calibration, these data open new opportunities to quantify LFMC for fire management applications. For this end, LFMC signal needs to be discriminated from atmospheric and topographic effects, sun and sensor geometry, soil background, species composition or other plant characteristics [11].

To compensate for some of these factors, several authors prefer to relate the LFMC dynamics to Relative Spectral Indices (relSI) [25–28]. The relSI normalize the SI for each pixel based on its values within a sufficiently large temporal series. The main goal of this study is to propose an operational spatially dynamic LFMC product including an herbaceous and woody layer ready for integration in fire behavior models. The product tests different Landsat-5 TM relSI normalized over 10+ year long time series. Finally, fire simulations with WFA demonstrate how LFMC impacts fire behavior, burned probability (BP) and fire growth.

2. Methods

2.1. Study Sites and Landsat-5 TM Data

This study selected nine chaparral sites for validation with a long Landsat-5 TM time series record and concurrent field LFMC sampling data from the National Fuel Moisture Database (NFMD, http://www.wfas.net/index.php/national-fuel-moisture-database-moisture-drought-103; last accessed 3 April, 2020). The LFMC data collection for the NFMC follows standard protocols, as described in Pollet and Brown [29]. Briefly, LFMC is obtained collecting samples at different heights on the shrubs and from different individuals [29].

The sites were in California and Oregon, within three Landsat-5 TM scenes across the Western US covering a wide range of environmental gradients (Figure 1; Table 1). Google Earth (Google Inc., 2013) visual inspection allowed the picking of sampling sites with no disturbance or rapid growth during the sampling period, and homogenous shrub cover of at least 1 km^2 as location of NFMD sites can be off by tens or hundreds of meters. Other site requirements were to have at least 20 Landsat-5 TM images with <10% cloud cover over at least six years that covered as much as possible of the phenological cycle of the species sampled. This work selected only field sampling dates within $\pm$6 days from image acquisition to reduce the impact of LFMC temporal variation between NFMD and Landsat-5 TM acquisition. LFMC data of the selected sites covered the whole fire season, from the beginning of spring until the end of the fall, although in some cases sampling was extended year-round.

Table 1. Description of the Live Fuel Moisture Content (LFMC) sampling sites and their Landsat-5 TM scene path and row.

Sites	Path	Row	Latitude (N)	Longitude(W)	Sampling period (yyyy/mm/dd)		Species	# Samples
Clark Motorway, Malibu	41	36	34.0844	118.8625	2001/01/08	2011/06/22	Big-pod buckbrush; Chamise	65
Glendora Rigde	41	36	34.1653	117.8650	2003/01/29	2011/10/28	Hoaryleaf ceanothus; Chamise	55
Laurel Canyon, Mt Olympus	41	36	34.1247	118.3689	2001/04/09	2011/10/28	Chamise	73
Trippet Ranch, Topanga	41	36	34.0933	118.5978	2001/02/05	2011/10/28	Chamise	69
Peach Motorway	41	36	34.3556	118.5347	2005/04/02	2011/10/28	Chamise	50

Placerita Canyon	41	36	34.3753	118.4389	2001/05/02	2011/10/28	Chamise	72
Kinsman	42	34	37.1981	119.4197	2001/09/20	2011/08/23	Whiteleaf Manzanita; Big-pod buckbrush	22
Keeney	42	29	43.9133	117.1783	2000/07/17	2011/08/30	Wyoming Big sagebrush	39
Shirttail	42	29	44.53	117.4186	2000/07/24	2011/09/16	Wyoming Big sagebrush	41

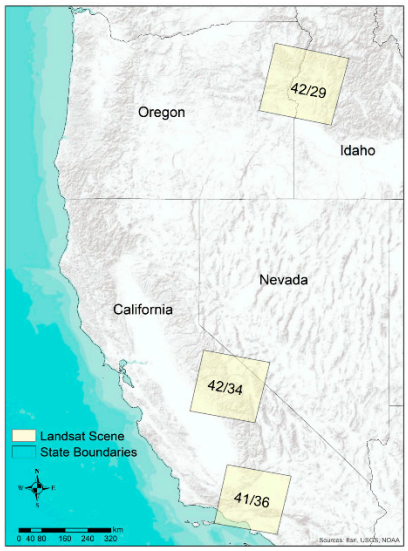

Figure 1. Landsat scenes corresponding to the study sites selected.

The Landsat Ecosystem Disturbance Adaptive Processing System (LEDAPS) provided orthorectified Landsat-5 TM surface reflectance data at 30 m spatial resolution through the United States Geological Survey (USGS) Earth Explorer web site (http://earthexplorer.usgs.gov/; last accessed 3 April, 2020). Their radiometric calibration involved the transformation of the digital numbers to at-sensor radiance, adjustment to top of atmosphere reflectance and atmospheric correction using the 6S radiative transfer model [30]. Landsat-5 TM scenes were clipped to the largest possible window containing data for the whole time series. In addition, the satellite overpass varies for each image acquisition. Therefore, a mask gave a -9999 value for all dates to the pixels out of the overpass in at least one image acquisition in the time series to ensure the same common pixels for all images in each scene. Further processing involved a topographic correction to reduce the differences in the time series due to sun illumination conditions and terrain. The Sun-Canopy-Sensor Correction with the C parameter (SCS+C) normalized reflectance (L_n) for this topographic factor [31] (Equation 1):

$$L_{n,b} = L_b \frac{\cos\alpha \cos\theta + C_b}{\cos i + C_b} \quad (1)$$

where L_b is the reflectance for each Landsat-5 TM band (b); α is the terrain slope; θ is the solar zenith angle; i is the incidence angle, which is the angle between the normal to the ground and the solar zenith; and C_b is the quotient between the slope and intercept of the linear regression equation between L_b and $\cos i$.

This study also tested Civco [32], C-Teillet [33] and smoothed C-Teillet [34] topographic corrections, but SCS+C worked best (results not shown), improving the relationship between the SI and the field LFMC when comparing before and after correcting the topographic effect. The SCS+C required a Digital Elevation Model (DEM) to perform the correction. The National Elevation Dataset delivered the DEM in grid float format at approximately 10 m spatial resolution

(https://www.usgs.gov/core-science-systems/ngp/tnm-delivery/; last accessed 3 April 2020). DEM mosaicking, reprojection to UTM 11 N WGS84 and nearest neighbor resampling to 30 m were necessary to match each Landsat-5 TM scene. Furthermore, SCS+C applied a different C_b parameter depending on the vegetation structure: herbaceous, shrub and forest. The 30 m National Land Cover from Fry et al. [35] provided the base map to reclassify 71–74 and 81 classes as herbaceous; 51–52 as shrubs; 41–43 as forest; and the rest as non-natural vegetation. Finally, a linear regression equation between L_b and $\cos i$ for all pixels in each of the four reclassified classes calculated C_b for each class.

2.2. Spectral Indices

LFMC prediction from Landsat-5 TM tested four SI previously used to retrieve LFMC (Table 2). The NDVI relates to LFMC only indirectly through changes in leaf pigments. It has successfully estimated LFMC, especially for grasslands [13,23]. The NDII predicted LFMC over Mediterranean environments [14,23,36]. NDII directly relates to LFMC through spectral changes occurring in the shortwave infrared (SWIR) region (band 5 in Landsat-5 TM), because of variability in the vegetation water content. The EVI estimated shrub LFMC successfully over chaparral vegetation with AVIRIS data [14,15,37]. EVI was originally designed for the MODIS sensor based on additional spectral bands than NDVI. Furthermore, it provides better sensitivity to high biomass while minimizing soil and atmosphere influences. The VARI estimated LFMC over chaparral [15,22]. VARI is indirectly related to LFMC through changes in leaf pigments.

Table 2. Spectral Indices (SI) selected to retrieve LFMC.

SI	Equation	
Normalized Difference Vegetation Index (NDVI) [38]	$\frac{\rho_{NIR} - \rho_R}{\rho_{NIR} + \rho_R}$	(2)
Normalized Difference Infrared Index (NDII) [39]	$\frac{\rho_{NIR} - \rho_{SWIR}}{\rho_{NIR} + \rho_{SWIR}}$	(3)
Enhanced Vegetation Index (EVI) [40]	$G\left(\frac{\rho_{NIR} - \rho_R}{\rho_{NIR} + C_1 * \rho_R - C_2 * \rho_B + L}\right)$	(4)
Visible Atmospherically Resistant Index (VARI) [41]	$\frac{\rho_G - \rho_R}{\rho_G + \rho_R - \rho_B}$	(5)

ρ_B, ρ_G, ρ_R, ρ_{NIR} and ρ_{SWIR} = blue, green, red, near infrared and shortwave infrared reflectance, respectively; G is a gain factor; C_1 and C_2 are the coefficients of the aerosol resistance term, and L is a soil-adjustment factor. These parameters have a value of 2.5, 6, 7.5 and 1, respectively.

Computing the relSI compensated differences among pixels in fractional cover, species composition, soil background and orientation among other factors in order to predict LFMC [25–28]. relSI is calculated as the difference between the SI at a specific time and the minimum SI (SI_{min}) in the temporal series for each pixel, divided by the difference between the maximum SI (SI_{max}) in the temporal series and SI_{min}. Newnham et al. [27] highlighted the importance of selecting an appropriate time interval and criteria to obtain the SI_{min} and SI_{max}. According to their findings, the time interval should be long enough to enable capturing the full range of spectral variation, but short enough to avoid capturing variation caused by land cover changes. The shortest period for the validation sites in Table 1 was six years, whereas the longest was eleven. The time frame covered the entire phenological vegetation cycle in all cases. Furthermore, the LEDAPS Landsat-5 TM product contained a mask that eliminated any cloud or cloud shadow pixel when searching for SI_{min} and SI_{max}. Finally, a similar normalization process from SI to relSI converted the field LFMC data to relative LFMC (relLFMC). As a result, minimum and maximum values by site compensated for differences in sampling methods and species composition across sites.

2.3. Landsat TM LFMC Product

This research applied an empirical method to estimate LFMC or relLFMC through linear interpolation from a SI or a relSI. These linear regression models are the traditional approach to relate

the spectral information derived from remotely sensed data and field measured LFMC [13,14,22]. Since the relEVI best predicted LFMC (see results section), it was the base for the Landsat-5 TM herbaceous and woody LFMC product. Pixels classified as shrubs or forest included herbaceous and woody LFMC layers whereas herbaceous pixels included only the herbaceous LFMC layer. To overcome the limitation of optical remote sensing not measuring the understory layer, a spring metaphor extrapolated the understory herbaceous values of the woody pixels from the surrounding herbaceous pixels using the "inpaint_nans" tool (https://www.mathworks.com/matlabcentral/fileexchange/4551-inpaint-nans, last accessed 3 April, 2020). This method adjusts a partial differential equation to extrapolate 2-dimesional data with springs that connect pixels to their neighbors in all directions. The performance of the method was evaluated by comparing a random extraction of 3000 herbaceous relEVI pixel values from April 16th, 2009 to the extrapolated results at these locations.

Information on fuel models based on the Scott and Burgan's [42] fire behavior fuel models classification version "LF 2014" with metadata "20161031" at 30 m resolution came from the LANDFIRE program. Fuel models classes were grouped into herbaceous, shrubs or forests according to their main fire carrier. The relEVI was understood as relLFMC and converted to absolute LFMC from the minimum and maximum field measured LFMC sampled in the Jasper Ridge Biological Preserve, CA(USA) using 30.0% to 197.2 % for herbaceous, 36.4% to 222.1 % for shrubs and 53.4% to 164.7% for forests [15]. Other scaling would be possible, but Jasper Ridge is preferred since field campaigns in Spring, Summer and Fall were carried out covering the phenological vegetation cycle, not only for shrubs, but also for herbaceous vegetation and forest. The nine chaparral sites from the NFMD had a minimum value of 43.5% and a maximum of 231.0% for shrubs. Hence, using Jasper Ridge data would introduce a small bias.

2.4. Fire Behavior Modeling with the LFMC Product

A 1000 by 1000 pixels window within the Landsat-5 TM Path 41 and Row 36 was used to test the differences in fire behavior due to LFMC. This site located Northwest of the city of Los Angeles includes part of Los Padres National Forest (Upper Left Corner: 119.115W 35.024N; Lower Right Corner: 118.781W 34.759N). WFA software was used to carry out the fire behavior simulations [19]. WFA provides real-time analysis of wildfire behavior and spread to directly support multi-agency wildfire incident management [43]. The semi-empirical fire spread model in WFA uses the Rothermel equations to model surface and crown fire behavior [44]. The model estimated how fires spread under different LFMC scenarios, keeping equal all other inputs. This is not a common approach in fire risk analysis, which usually uses stochastic inputs. However, the goal here was to assess the difference in behavior only due to LFMC.

The simulations calculated fireline intensity, Flame Length (FL) and Rate of Spread (ROS) at the 30 m pixel level resolution, considering the maximum potential fire behavior in each pixel [45]. In addition, WFA predicted the independent spread of 111,559 fires with a duration of eight hours with a 90 by 90 m ignition point every three pixels in all directions. The hourly burned area quantified the impact of each fire simulation on the landscape. After running all the fire simulations, WFA calculated the output BP that represents the amount of times the fires reached each pixel.

Modeling fire behavior and spread required several spatial-temporal inputs: the DEM already used for the topographic correction, Scott and Burgan's fuel models used to generate the LFMC product described above, a constant moderate wind speed at 20 feet of 11 km/h at a 45º direction from Northeast to Southwest as well as constant Dead Fuel Moisture Content (DFMC) values of 5%, 7% and 9% for 1, 10 and 100 h fuels, respectively.

Simulations considered four LFMC scenarios: a constant overall median LFMC value of 99% for herbaceous, 129% for shrubs and 109% for forest from Jasper Ridge field data; a constant overall tenth percentile LFMC value of 30% for herbaceous, 55% for shrubs and 65% for forest also from Jasper Ridge field data; and the LFMC product generated with the relEVI from Landsat-5 TM data on 16 April 2009 and 25 October 2009. The median and tenth percentile were calculated considering the minimum and maximum values of all samples collected in Jasper Ridge for each vegetation type [15].

The Landsat-5 TM dates were selected since they would represent two distinct LFMC scenarios, in spring and end of the summer/beginning of autumn. Note also that according to Rothermel's surface fire behavior model, herbaceous LFMC is cured at 30% and woody LFMC enters dormancy at 60% [42,46].

3. Results

The EVI presented the highest r and the lowest RMSE with the field measured LFMC for five out of the nine validation sites (Table 3). When all sites were considered together, a significant drop in r and an increase in RMSE was observed, with the highest r value as low as 0.44% and the lowest RMSE as high as 33.35 % for EVI. The relationship between LFMC and SI for all sites improved after using relLFMC and relSI, increasing r up to 0.69% and decreasing the RMSE to 19% for relEVI, which was again the best predictive variable.

The relEVI was thus used to predict the herbaceous and woody LFMC from Landsat-5 TM data on 16th of April and on 25th of October (Figure 2), to analyze fire behavior through WFA simulations. The extrapolation algorithm to estimate the understory herbaceous LFMC of the woody pixels was tested over a random set of overstory herbaceous pixels. The comparison between their actual herbaceous relEVI values and the extrapolated ones yielded r = 0.94 and RMSE = 7.43%.

Table 3. r and Root Mean Square Error (RMSE) between field measured LFMC/relLFMC and SI/relSI. All r are statistically significant (*P*-value < 0.001).

			r				RMSE (%)			
Site	**Depen. Var.**	**Indep. Var.**	**NDVI**	**NDII**	**EVI**	**VARI**	**NDVI**	**NDII**	**EVI**	**VARI**
ClarkMotorway,Malibu	LFMC	SI	0.85	0.77	**0.89**	0.65	15.39	18.29	**13.07**	22.05
Glendora Ridge, Glendora	LFMC	SI	0.69	0.65	**0.80**	0.33	19.38	20.30	**16.03**	25.17
Laurel Canyon	LFMC	SI	0.81	0.85	**0.87**	0.48	15.53	13.95	**13.11**	23.46
Trippet Ranch	LFMC	SI	**0.84**	0.72	0.77	0.73	**26.33**	33.80	31.39	33.57
Peach Motorway	LFMC	SI	0.87	0.89	**0.93**	0.79	11.67	10.44	**8.72**	14.50
Placerita Canyon	LFMC	SI	0.80	0.84	**0.86**	0.52	20.24	18.32	**17.30**	28.91
Kinsman	LFMC	SI	0.66	**0.82**	**0.82**	0.61	17.60	**13.28**	13.40	18.54
Keeney	LFMC	SI	**0.79**	0.64	0.74	0.36	**22.02**	27.61	24.11	33.58
Shirttail	LFMC	SI	**0.73**	0.67	0.69	0.69	**24.48**	26.53	26.12	26.23
All sites	LFMC	SI	0.22	0.32	**0.44**	0.35	36.26	35.16	33.35	34.85
All sites	relLFMC	SI	0.46	0.52	**0.62**	0.50	0.24	0.23	**0.21**	0.23
All sites	LFMC	relSI	0.49	0.51	**0.57**	0.49	32.47	32.00	**30.51**	32.31
All sites	relLFMC	relSI	0.61	0.66	**0.69**	0.55	0.21	0.20	**0.19**	0.22

The average LFMC value based on relEVI for 16th of April 2009 was closer to the constant median LFMC map (Figure 2), whereas the one for 25th of October 2009 was closer to the constant tenth percentile LFMC map. These constant LFMC values could be used as a baseline for comparison. It is evident that this approach cannot capture the spatial variability of LFMC across the landscape as the relEVI maps do. For example, herbaceous LFMC for 16th of April on the Northern part of Figure 2 was generally below the median LFMC map, but the Southern part was above it. Instead, herbaceous LFMC for 25th of October was generally like the tenth percentile LFMC map, except for the Southwestern part where it was higher. In the case of the woody for 16th of April, the Eastern part was higher than the median, but the Western part was lower. In contrast, woody LFMC for 25th of October was generally like the tenth percentile LFMC map, but with randomly distributed patches having higher LFMC (Figure 2).

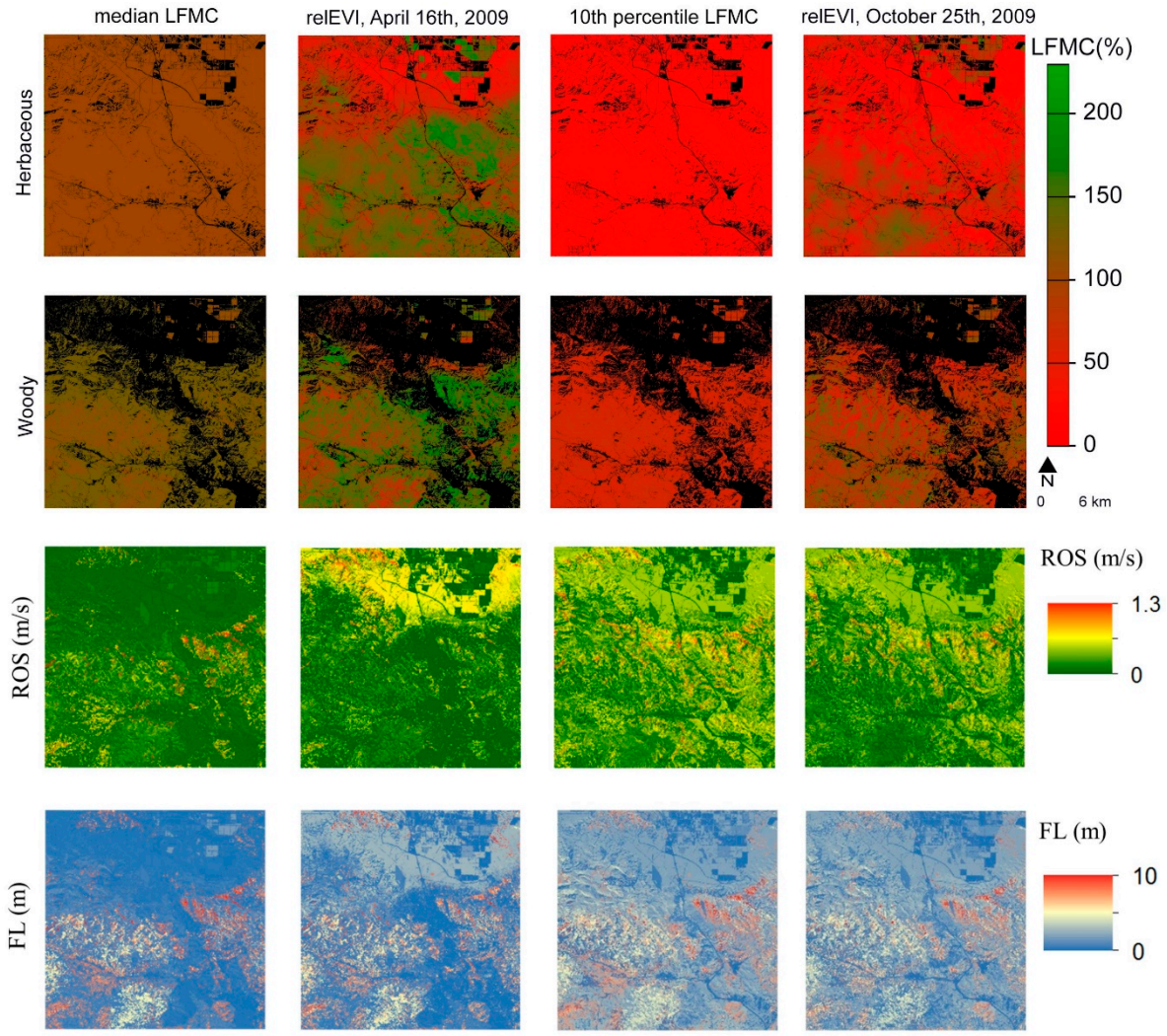

Figure 2. Herbaceous and woody LFMC products from a constant median and tenth percentile LFMC, and from Landsat-5 TM relEVI data on April 16th and on October 25th of 2009 and estimated fire behavior for each scenario in terms of ROS and FL.

The LFMC products from Figure 2 caused differences in the fire simulations performed on WFA (Figures 2, 3 and 4). All input variables in the simulations were the same except the herbaceous and woody LFMC layers. Despite this, the differences in fire behavior (both ROS and FL; Figure 2), average burned area per fire (Figure 3) and BP (Figure 4) were significant and increased with the time since ignition. Results based on 16th of April and 25th of October LFMC fell in between the minimum value of the tenth percentile and the maximum of the median LFMC (Figure 3). We observed spatial differences in terms of ROS and FL among the LFMC products (Figure 1). For instance, the ROS for 16th of April was higher in the northern part of the study area than in the southern part, whereas this pattern was the inverse for other scenarios such as 25th of October, suggesting the importance of considering the spatial variability of LFMC in operational environments. These results are consistent with the BP outputs (Figure 4), given that the areas with higher BP values also had higher ROS. BP maps derived using the tenth percentile and relEVI for the 25th of October, showed similar spatial distribution (Figure 4), although higher BP values where obtained for the former which resulted in an average difference in burned area greater than 30 ha 8 h after ignition (21% and 36% higher than the burned area for the relEVI 25th of October and 16th of April, respectively). Differences in the spatial distribution in BP maps were more evident when comparing the relEVI maps for 16th of April to the constant median LFMC value.

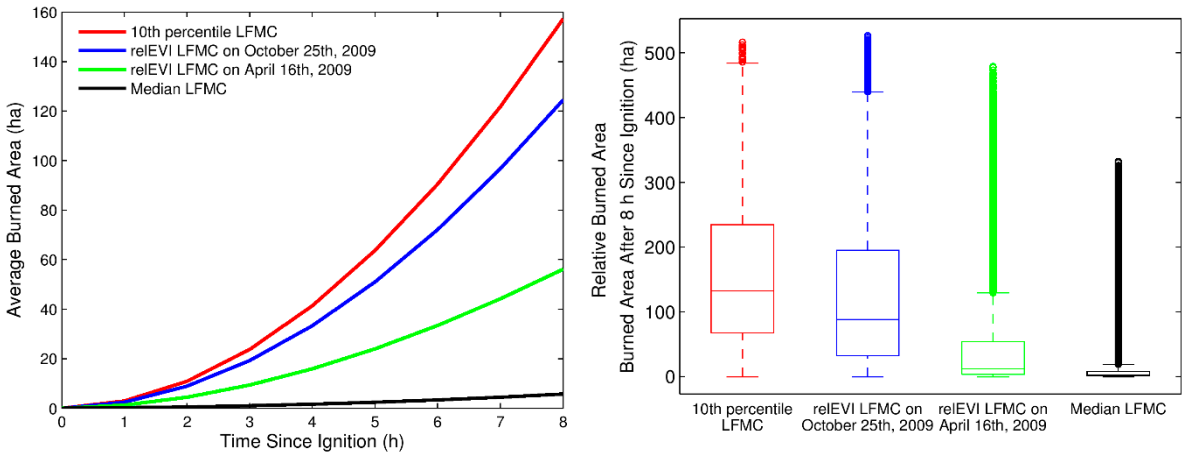

Figure 3. Average burned area after time since ignition for fire simulations and boxplots of the burned area 8-hours after ignition in Wildfire Analyst (WFA) with the different LFMC scenarios from Figure 2.

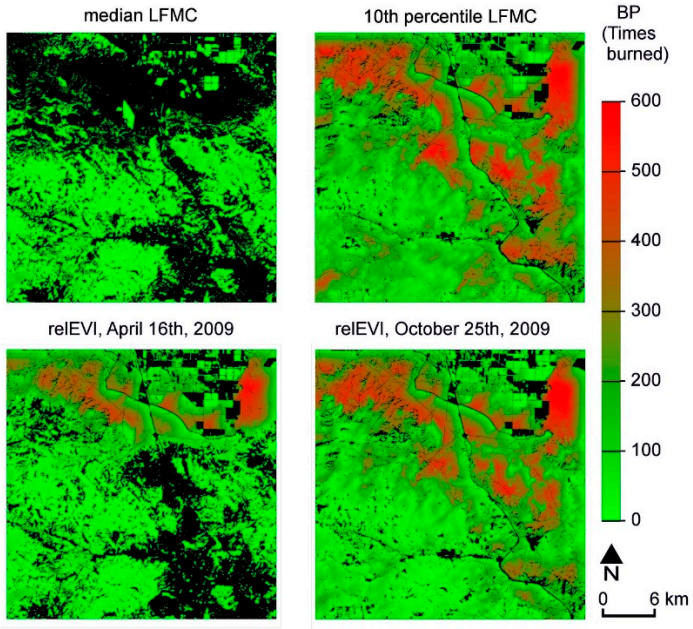

Figure 4. Burned probability (BP) maps of the fire simulations in WFA with the different LFMC scenarios from Figure 2.

4. Discussion

Many other studies have estimated LFMC from optical remote sensing [11], including Landsat-5 TM data [23]. The novelty of the Landsat-5 TM relEVI LFMC product generated in this study is that it provides an herbaceous and woody layer that can be integrated into fire behavior models like WFA. This integration produces spatial differences in fire behavior (ROS, FL and fireline intensity) and subsequently, BP and average burned area, compared to using a constant LFMC value (Figure 4). The reason to choose Landsat-5 TM data was its long time series, coinciding with field data in the NFMD for validation. However, the application of this approach to Landsat-7 and -8 and Sentinel-2A and -2B should be possible in order to generate systematic products at 10–30 m spatial resolution. Such products will improve those from MODIS-like sensors with >250 m spatial resolution in terms of operational adoption [18]. Given its higher temporal resolution, MODIS like sensors could also be used for gap filling [47]. However, such a product would require proper sensor inter-calibration to

determine the spectral band adjustment factors. This should not only be done over pseudo-invariant calibration sites, as diverse studies have demonstrated that these cross-sensor adjustment factors are land cover dependent [48,49]. Besides, the compensation of solar illumination due to the irregular shape of the terrain of a topographic correction is also necessary.

Correlations between LFMC and SI in Table 3 were much higher at individual sites than when all sites were considered together. This agrees with Roberts et al. [14] results for the Santa Monica Mountains, an area enclosed within the Landsat-5 TM scene 41/26 used in this study. Stow et al. [22] also found a decrease in correlation between LFMC and VARI for San Diego County using MODIS data, when data from different sampling sites were pooled together. The different species sampled, time since disturbance, sampling method, time of the year and the variety of environmental factors affecting the vegetation of each sampling site can explain the significant drop in regression values when all sites were considered together. In addition, it should be considered that LFMC is a function of leaf age and leaf chemistry [50,51].

As Roberts et al. [14] pointed out, sampling methodology, site quality and plant functional type are important factors affecting the relation between the LFMC and the information derived from remote sensing, and can significantly vary from one site to another. These factors limit reaching a RMSE below 20% here (Table 3) and also in other studies [11]. For example, the NFMD field collections might not always be at the exact same location or a sample might not be representative of the surrounding LFMC within a pixel, as NFMD samples where not collected with the objective to be representative of a 30 m pixel. Specifically, sites in Table 1 did not contain available information on the sampling procedure used, the number of individuals sampled, the proportion of twigs/leaves and new/old leaves sampled, species proportion in the case of mixed shrublands, or the fractional cover for each site. Additionally, phenological differences among the species and sites could have affected the correlation values. In fact, SI from two study sites in scene 42/29 (Keeney and Shirttail) showed lower values than found in the other two scenes used. Roberts et al. [14] found a linear relationship between LFMC values and different SI when LFMC surpassed 60%. Despite also using a linear model here, a non-linear relationship worked slightly better for many sites due to the large inter-annual variability that spanned over 10 years.

Data normalization significantly improved the results as the effect of varying vegetation cover and type was reduced. These results agree with Stow and Niphadkar [28], who obtained a better coefficient of determination for models applying relSI to estimate LFMC using MODIS data. A clear improvement in the correlations was observed in Table 3 when LFMC values were also normalized by site. The long period of LFMC measurements available for each study site allowed the capture of the full range of LFMC variation. This suggests that the normalization of field LFMC values reduces the effect of environmental factors affecting field measured LFMC values and thus, to better capture the LFMC dynamics of the vegetation. This is a unique aspect of this study, as other studies only normalized SI but not LFMC [22,23]. The normalization of field measured LFMC values might hamper obtaining the absolute LFMC value for those pixels where no field measurements are available. Yet, it should still be possible to detect LFMC anomalies, such as for example when the fuel is cured or dormant.

Out of the four vegetation indices tested, VARI showed the poorest performance. These results contrast with those obtained by Stow et al. [22], Roberts et al. [14], Dennison et al. [52] and Casas et al. [15] who found VARI as the best performing index to estimate LFMC in similar environments. The different spectral and spatial sensor resolutions might explain the differences between these studies and results presented here with Landsat-5 TM data. Nevertheless, Roberts et al. [14] found a similar performance between NDVI, EVI, NDII and VARI using AVIRIS data with a spatial resolution of 20 m. Regarding the effect of the spectral resolution, Casas et al. [15] tested multiple band combinations with AVIRIS data and showed how LFMC was significantly affected by the band combination selected. Translated to broadband sensors, this means that the center wavelength and band-width of the sensors can affect the estimation of LFMC, despite being in the same spectral region.

The NFMD served for validation of the LFMC product over the shrub canopy woody layer, but the herbaceous and forest canopy woody layer lacks validation here. Nevertheless, a global validation

from MODIS demonstrated that relEVI is a reliable LFMC estimator [53]. In addition, many other previous studies have also demonstrated that optical remote sensing predicts herbaceous LFMC with better accuracy than for shrubs, due to a simpler canopy structure and higher temporal LFMC variation [17,18,23]. To the contrary, the forest canopy woody layer shares the space with the understory shrub and herbaceous canopy. Their deeper tree root system reduces the temporal variation in evergreen forest LFMC. These complexities make the canopy the hardest layer to validate, producing poorer accuracy than for shrubs [15,18]. Furthermore, sampling the forest canopy is also challenging due to the canopy height, which requires the use of techniques such as a shot throw-line launcher [54]. Shorter crop trees without understory produce stronger relationships between optical remote sensing and canopy water content [55,56]. This latter variable relates to LFMC after accounting for specific leaf area and leaf area index [57]. Another remarkable aspect is that forest canopy LFMC (foliar moisture) becomes important for crown fire modeling but not for surface fires [58].

Extrapolating to the understory herbaceous LFMC on the woody pixels from the surrounding herbaceous pixels rendered a strong relationship ($r = 0.94$) on a random sample, compared to their actual herbaceous relEVI values. Nevertheless, further testing is needed to demonstrate how the extrapolation algorithm works over a sample set with larger gaps of herbaceous pixels. Moreover, the herbaceous LFMC under the woody layer should be slightly higher than when it is the top canopy layer, and hence sun exposed. This correction factor remains to be explored.

Despite these limitations, a continuous sampling from direct satellite observations assures capture of the spatial LFMC variability across the landscape. After proper testing on actual fires, this spatially dynamic information could be integrated into fire behavior models like WFA. This approach should improve fire behavior estimation and progression over using constant LFMC values for each vegetation layer or fuel model (Figure 4) as shown in this work. These improvements would reduce errors in fire event duration, resulting in better real time fire analyses of the fire progression. Furthermore, improved fire simulations considering the spatial effect of LFMC would help in enhancing the estimation of important outputs, such as the annual BP and fire behavior for fire risk assessment. Products based on extrapolation from field or meteorological data alone should help to adjust the systematic relEVI LFMC from direct satellite observations. The NFMD dataset collects direct LFMC measurements, but with a limited temporal and spatial coverage. Based on this field data, the minimum and maximum thresholds to convert relEVI to LFMC could be modified. Meteorological phenological models like Jolly et al. [20] have the advantage of providing hourly herbaceous and woody LFMC. The limitation of this method is that it estimates indirectly LFMC from a model and requires a large meteorological network for an accurate spatial extrapolation. Another complement to optical data is using radar sensors like Sentinel 1 or the NASA-ISRO Synthetic Aperture Radar (NISAR), the later to be launched in 2021. Radar is sensitive to the water in whole canopy layer rather than the top layer observed from optical data [59]. Therefore, it requires untangling between the soil moisture, water in trunks and branches, herbaceous LFMC and woody LFMC.

5. Conclusions

This study generated spatially dynamic maps of herbaceous and woody LFMC from relEVI Landsat-5 TM data that could be integrated in fire behavior simulators like WFA. Before this, it would be beneficial to test it on simulations of actual fires. Since optical remote sensing only detects the top layer, it requires extrapolating to the understory herbaceous LFMC on the woody pixels from the surrounding herbaceous pixel. Landsat-5 TM long time series served for validating the LFMC, over the shrub that is the main fire carrier. The LFMC product alone compared to constant LFMC significantly impacts the fire spatial distribution in terms of BP and average burned area, when simulating fires in WFA with the same values for all other input variables in the simulation. Based on this analysis over Landsat-5 TM, a Landsat-7 and -8 and Sentinel-2A and -2B product seems feasible. This means a systematic product at 10–30 m spatial resolution that requires proper sensor inter-calibration and topographic correction. Such a product would benefit from adjustment with

field and meteorological data and integration with coarser spatial resolution with higher temporal observations like MODIS and radar sensors like upcoming NISAR.

The evaluation of different SI to estimate LFMC and its dynamics in the Western US concluded that EVI generally performs the best, followed by NDII, NDVI and VARI. While all SI presented good relationships for each individual sampling site, there was a significant drop when sites were pooled together. Normalizing the data improved the results overcoming the effect of varying vegetation cover and type on the signal recorded by the sensor. In addition, relative LFMC values account for the dynamics rather than the absolute LFMC variation, which can help to detect LFMC anomalies and thus, detect when the fuel is cured or dormant.

Author Contributions: Conceptualization, M.G., D.R., M.Y., J.S., A.C., S.M., M.M., L.V., J.G., S.U.; methodology, M.G., D.R., M.Y., J.S., A.C, J.R., M.M., L.V., J.G., S.U.; writing-original draft, M.G., D.R.; writing-review and editing, M.G., D.R., M.Y., J.S., A.C, S.M., J.R., M.M., L.V., J.G., S.U.; supervision, D.R., M.Y., J.S., S.M., J.R., M.M., L.V., J.G., S.U.; visualization, M.G., D.R.; formal analysis, M.G., D.R., A.C; investigation, M.G., D.R.; validation, M.G., D.R.; funding acquisition, D.R., S.U.; project administration, S.U. All authors have read and agreed to the published version of the manuscript.

Funding: NASA NNX11AF93G: The European Union SENSORVEG (FP7-PEOPLE-2009-IRSES-246666); and the Spanish Ministry of Economy and Competitiveness SynerTGE (CGL2015-G9095-R-MINECO/FEDER, EU) funded this research. In addition, a CONICYT Doctoral Fellowship from the Chilean Government supported J.G.

Acknowledgments: We thank the United States Forest Service for making the field LFMC available and the United States Geological Survey for the Landsat-5 TM data.

Conflicts of Interest: The authors declare no conflict of interest.

References

1. Koutsias, N.; Karteris, M. Classification analyses of vegetation for delineating forest fire fuel complexes in a Mediterranean test site using satellite remote sensing and GIS. *Int. J. Remote Sens.* **2003**, *24*, 3093–3104, doi:10.1080/0143116021000021152.
2. Burgan, R.E.; Rothermel, R.C. *BEHAVE: Fire Behavior Prediction and Fuel Modeling System. Fuel Subsystem*; GTR INT-167; USDA Forest Service: Ogden, Utah, 1984.
3. Anderson, S.A.J.; Anderson, W.R. Ignition and fire spread thresholds in gorse (Ulex europaeus). *Int. J. Wildland Fire* **2010**, *19*, 589–598, doi:10.1071/WF09008.
4. Finney, M.A. *FARSITE: Fire Area Simulator—Model development and evaluation*; RMRS-RP-4; USDA Forest Service, Rocky Mountain Research Station: Ogden, UT, USA, 1998; p. 47.
5. Viegas, D.X.; Viegas, T.P.; Ferreira, A.D. Moisture content of fine forest fuels and fire occurrence in central Portugal. *Int. J. Wildland Fire* **1992**, *2*, 69–85, doi:10.1071/WF9920069.
6. Pimont, F.; Ruffault, J.; Martin-StPaul, N.K.; Dupuy, J.-L. Why is the effect of live fuel moisture content on fire rate of spread underestimated in field experiments in shrublands? *Int. J. Wildland Fire* **2019**, *28*, 127–137, doi:10.1071/WF18091.
7. Plucinski, M.P.; Anderson, W.R.; Bradstock, R.A.; Gill, A.M. The initiation of fire spread in shrubland fuels recreated in the laboratory. *Int. J. Wildland Fire* **2010**, *19*, 512–520, doi:10.1071/WF09038.
8. Matthews, S. Effect of drying temperature on fuel moisture content measurements. *Int. J. Wildland Fire* **2010**, *19*, 800–802, doi:10.1071/WF08188.
9. NWCG. *User Guide for the Glossary of Wildland Fire*; PMS 937; 2018, https://www.nwcg.gov/publications/937.
10. Garcia, M.; Litago, J.; Palacios-Orueta, A.; Pinzon, J.E.; Ustin, S. Short-term propagation of rainfall perturbations on terrestrial ecosystems in central California. *Appl. Veg. Sci.* **2010**, *13*, 146–162, doi:10.1111/j.1654-109X.2009.01057.x.
11. Yebra, M.; Dennison, P.E.; Chuvieco, E.; Riaño, D.; Zylstra, P.; Hunt, E.R.J.; Danson, F.M.; Qi, Y.; Jurdao, S. A global review of remote sensing of live fuel moisture content for fire danger assessment: Moving towards operational products. *Remote Sens. Environ.* **2013**, *136*, 455–468, doi:10.1016/j.rse.2013.05.029.
12. Dennison, P.E.; Roberts, D.A.; Thorgusen, S.R.; Regelbrugge, J.C.; Weise, D.; Lee, C. Modeling seasonal changes in live fuel moisture and equivalent water thickness using a cumulative water balance index. *Remote Sens. Environ.* **2003**, *88*, 442–452, doi:10.1016/j.rse.2003.08.015.

13. Garcia, M.; Chuvieco, E.; Nieto, H.; Aguado, I. Combining AVHRR and meteorological data for estimating live fuel moisture content. *Remote Sens. Environ.* **2008**, *112*, 3618–3627, doi:10.1016/j.rse.2008.05.002.
14. Roberts, D.A.; Dennison, P.E.; Peterson, S.; Sweeney, S.; Rechel, J. Evaluation of airborne visible/infrared imaging spectrometer (AVIRIS) and moderate resolution imaging spectrometer (MODIS) measures of live fuel moisture and fuel condition in a shrubland ecosystem in southern California. *J. Geophys. Res. Biogeosci.* **2006**, *111*, doi:10.1029/2005JG000113.
15. Casas, A.; Riaño, D.; Ustin, S.L.; Dennison, P.; Salas, J. Estimation of water-related biochemical and biophysical vegetation properties using multitemporal airborne hyperspectral data and its comparison to MODIS spectral response. *Remote Sens. Environ.* **2014**, *148*, 28–41, doi:10.1016/j.rse.2014.03.011.
16. Jurdao, S.; Yebra, M.; Guerschman, J.P.; Chuvieco, E. Regional estimation of woodland moisture content by inverting Radiative Transfer Models. *Remote Sens. Environ.* **2013**, *132*, 59–70, doi:10.1016/j.rse.2013.01.004.
17. Yebra, M.; Chuvieco, E.; Riaño, D. Estimation of live Fuel Moisture Content from MODIS images for fire risk assessment. *Agr. For. Meteorol.* **2008**, *148*, 523–536, doi:10.1016/j.agrformet.2007.12.005.
18. Yebra, M.; Quan, X.; Riaño, D.; Rozas Larraondo, P.; van Dijk, A.; Cary, G.J. A fuel moisture content and flammability monitoring methodology for continental Australia based on optical remote sensing. *Remote Sens. Environ.* **2018**, *212*, 260–272, doi:10.1016/j.rse.2018.04.053.
19. Ramirez, J.; Monedero, S.; Buckley, D. New approaches in fire simulations analysis with Wildfire Analyst. In Proceedings of The 5th International Wildland Fire Conference, Sun City, South Africa, 9–13 May 2011.
20. Jolly, W.M.; Nemani, R.; Running, S.W. A generalized, bioclimatic index to predict foliar phenology in response to climate. *Global Chang. Biol.* **2005**, *11*, 619–632, doi:10.1111/j.1365-2486.2005.00930.x.
21. Chuvieco, E.; Cocero, D.; Riaño, D.; Martin, P.; Martínez-Vega, J.; de la Riva, J.; Pérez, F. Combining NDVI and Surface Temperature for the estimation of live fuels moisture content in forest fire danger rating. *Remote Sens. Environ.* **2004**, *92*, 322–331, doi:10.1016/j.rse.2004.01.019.
22. Stow, D.; Niphadkar, M.; Kaiser, J. MODIS-derived visible atmospherically resistant index for monitoring chaparral moisture content. *Int. J. Remote Sens* **2005**, *26*, 3867–3873, doi:10.1080/01431160500185342.
23. Chuvieco, E.; Riaño, D.; Aguado, I.; Cocero, D. Estimation of fuel moisture content from multitemporal analysis of Landsat Thematic Mapper reflectance data: Applications in fire danger assessment. *Int. J. Remote Sens.* **2002**, *23*, 2145–2162, doi:10.1080/01431160110069818.
24. Whitcraft, A.K.; Becker-Reshef, I.; Killough, B.D.; Justice, C.O. Meeting Earth Observation Requirements for Global Agricultural Monitoring: An Evaluation of the Revisit Capabilities of Current and Planned Moderate Resolution Optical Earth Observing Missions. *Remote Sens.* **2015**, *7*, 1482–1503, doi:10.3390/rs70201482.
25. Burgan, R.E.; Hartford, R.A. *Monitoring Vegetation Greenness with Satellite Data*; GTR INT-297; USDA Forest Service: Ogden, UT, USA, 1993.
26. Caccamo, G.; Chisholm, L.A.; Bradstock, R.A.; Puotinen, M.L.; Pippen, B.G. Monitoring live fuel moisture content of heathland, shrubland and sclerophyll forest in south-eastern Australia using MODIS data. *Int. J. Wildland Fire* **2012**, *21*, 257–269, doi:10.1071/WF11024.
27. Newnham, G.J.; Verbesselt, J.; Grant, I.F.; Anderson, S.A.J. Relative Greenness Index for assessing curing of grassland fuel. *Remote Sens. Environ.* **2011**, *115*, 1456–1463, doi:10.1016/j.rse.2011.02.005.
28. Stow, D.; Niphadkar, M. Stability, normalization and accuracy of MODIS-derived estimates of live fuel moisture for southern California chaparral. *Int. J. Remote Sens.* **2007**, *28*, 5175–5182, doi:10.1080/01431160701616129.
29. Pollet, J.; Brown, A. *Fuel Moisture Sampling Guide*; Bureau of Land Management: Utah State Office, Salt Lake City, UT, USA, 2007.
30. Masek, J.G.; Vermote, E.F.; Saleous, N.E.; Wolfe, R.; Hall, F.G.; Huemmrich, K.F.; Gao, F.; Kutler, J.; Lim, T.-K. A Landsat surface reflectance dataset for North America, 1990-2000. *IEEE Geosci. Remote Sens. Lett.* **2006**, *3*, doi:10.1109/LGRS.2005.857030.
31. Soenen, S.A.; Peddle, D.R.; Coburn, C.A. SCS+C: A modified sun-canopy-sensor topographic correction in forested terrain. *IEEE Trans. Geosci. Remote* **2005**, *43*, 2148–2159, doi:10.1109/TGRS.2005.852480.
32. Civco, D.L. Topographic Normalization of Landsat Thematic Mapper Digital Imagery. *Photogramm. Eng. Remote Sens.* **1989**, *55*, 1303–1309.
33. Teillet, P.M.; Guindon, B.; Goodeonugh, D.G. On the slope-aspect correction of multispectral scanner data. *Can. J. Remote Sens.* **1982**, *8*, 84–106, doi:10.1080/07038992.1982.10855028.

34. Riaño, D.; Chuvieco, E.; Salas, F.J.; Aguado, I. Assessment of different topographic corrections in Landsat-TM data for mapping vegetation types. *IEEE Trans. Geosci. Remote* **2003**, *41*, 1056–1061, doi:10.1109/TGRS.2003.811693.
35. Fry, J.A.; Xian, G.; Jin, S.; Dewitz, J.A.; Homer, C.G.; Yang, L.; Barnes, C.A.; Herold, N.D.; Wickham, J.D. Completion of the 2006 national land cover database for the conterminous united states. *Photogramm. Eng. Remote Sens.* **2011**, *77*, 858–864.
36. Danson, F.M.; Steven, M.D.; Malthus, T.J.; Clark, J.A. High-espectral resolution data for determining leaf water content. *Int. J. Remote Sens.* **1992**, *13*, 461–470, doi:10.1080/01431169208904049.
37. Mendiguren, G.; Martin, M.P.; Nieto, H.; Pacheco-Labrador, J.; Jurdao, S. Seasonal variation in grass water content estimated from proximal sensing and MODIS time series in a Mediterranean Fluxnet site. *Biogeosciences* **2015**, *12*, 5523–5535, doi:10.5194/bg-12-5523-2015.
38. Tucker, C.J. Red and photographic infrared linear combinations for monitoring vegetation. *Remote Sens. Environ.* **1979**, *8*, 127–150, doi:10.1016/0034-4257(79)90013-0.
39. Hunt, E.R.; Rock, B.N. Detection of changes in leaf water content using near and middle-infrared reflectances. *Remote Sens. Environ.* **1989**, *30*, 43–54, doi:10.1016/0034-4257(89)90046-1.
40. Huete, A.; Didan, K.; Miura, T.; Rodriguez, E.P.; Gao, X.; Ferreira, L.G. Overview of the radiometric and biophysical performance of the MODIS vegetation indices. *Remote Sens. Environ.* **2002**, *83*, 195–213, doi:10.1016/S0034-4257(02)00096-2.
41. Gitelson, A.A.; Kaufman, Y.J.; Stark, R.; Rundquist, D. Novel algorithms for remote estimation of vegetation fraction. *Remote Sens. Environ.* **2002**, *80*, 76–87, doi:10.1016/S0034-4257(01)00289-9.
42. Scott, J.H.; Burgan, R.E. *Standard Fire Behavior Fuel Models: A Comprehensive Set for Use with Rothermel's Surface fire Spread Model*; U.S. Department of Agriculture, Forest Service, Rocky Mountain Research Station: Fort Collins, CO, USA, 2005; p. 72.
43. Monedero, S.; Ramirez, J.; Molina-Terren, D.; Cardil, A. Simulating wildfires backwards in time from the final fire perimeter in point-functional fire models. *Environ. Modell. Softw.* **2017**, *92*, 163–168, doi:10.1016/j.envsoft.2017.02.023.
44. Rothermel, R.C. *A Mathematical Model for Predicting Fire Spread in Wildland Fuels*; Research Paper INT-115; USDA, Forest Service: Ogden, UT, USA, 1972.
45. Finney, M. An overview of FlamMap fire modeling capabilities. In Proceedings of Fuels Management—How to Measure Success: Conference Proceedings, Portland, OR, USA, 28–30 March 2006; pp. 213–220.
46. Rothermel, R.C. *How to Predict the Spread and Intensity of Forest and Range Fires*; GTR INT-143; USDA, Forest Service: Ogden, UT, USA, 1983; p. 161.
47. Emelyanova, I.V.; McVicar, T.R.; Van Niel, T.G.; Li, L.T.; van Dijk, A.I.J.M. Assessing the accuracy of blending Landsat–MODIS surface reflectances in two landscapes with contrasting spatial and temporal dynamics: A framework for algorithm selection. *Remote Sens. Environ.* **2013**, *133*, 193–209, doi:10.1016/j.rse.2013.02.007.
48. D'Odorico, P.; Gonsamo, A.; Damm, A.; Schaepman, M.E. Experimental Evaluation of Sentinel-2 Spectral Response Functions for NDVI Time-Series Continuity. *IEEE Trans. Geosci. Remote* **2013**, *51*, 1336–1348, doi:10.1109/TGRS.2012.2235447.
49. Li, P.; Jiang, L.; Feng, Z. Cross-Comparison of Vegetation Indices Derived from Landsat-7 Enhanced Thematic Mapper Plus (ETM plus) and Landsat-8 Operational Land Imager (OLI) Sensors. *Remote Sens.* **2014**, *6*, 310–329, doi:10.3390/rs6010310.
50. Qi, Y.; Dennison, P.E.; Jolly, W.M.; Kropp, R.C.; Brewer, S.C. Spectroscopic analysis of seasonal changes in live fuel moisture content and leaf dry mass. *Remote Sens. Environ.* **2014**, *150*, 198–206, doi:10.1016/j.rse.2014.05.004.
51. Qi, Y.; Jolly, W.M.; Dennison, P.E.; Kropp, R.C. Seasonal relationships between foliar moisture content, heat content and biochemistry of lodgepole line and big sagebrush foliage. *Int. J. Wildland Fire* **2016**, *25*, 574–578, doi:10.1071/wf15156.
52. Dennison, P.E.; Moritz, M.A.; Taylor, R.S. Evaluating predictive models of critical live fuel moisture in the Santa Monica Mountains, California. *Int. J. Wildland Fire* **2008**, *17*, 18–27, doi:10.1071/WF07017.
53. Yebra, M.; Riaño, D.; Quan, X.; Mouillot, F.; Paget, E.; Di Bella, C.M.; García, M.; Martín, P.; van Dijk, A.; Cary, G.J.; et al. Global validation of Live Fuel Moisture Content (LFMC) products from satellite MODIS. In Proceedings of 5th International Symposium Recent Advances in Quantitative Remote Sensing Torrent (Valencia), Spain, 18–22 September 2017.

54. Youngentob, K.N.; Zdenek, C.; van Gorsel, E. A simple and effective method to collect leaves and seeds from tall trees. *Methods Ecol. Evolution* **2016**, *7*, 1119–1123, doi:10.1111/2041-210X.12554.
55. Cheng, T.; Riaño, D.; Ustin, S.L. Detecting diurnal and seasonal variation in canopy water content of nut tree orchards from airborne imaging spectroscopy data using continuous wavelet analysis. *Remote Sens. Environ.* **2014**, *143*, 39–53, doi:10.1016/j.rse.2013.11.018.
56. Cheng, T.; Riaño, D.; Koltunov, A.; Whiting, M.L.; Ustin, S.L.; Rodriguez, J.M. Detection of diurnal variation in orchard canopy water content using MODIS/ASTER airborne simulator (MASTER) data. *Remote Sens. Environ.* **2013**, *132*, 1–12, doi:10.1016/j.rse.2012.12.024.
57. Ustin, S.L.; Riaño, D.; Hunt, E.R., Jr. Estimating Canopy Water Content from Spectroscopy. *Isr. J. Plant Sci.* **2012**, *60*, 9–23, doi:10.1560/IJPS.60.1-2.9.
58. Alexander, M.E.; Cruz, M.G. Assessing the effect of foliar moisture on the spread rate of crown fires. *Int. J. Wildland Fire* **2013**, *22*, 415–427, doi:10.1071/wf12008.
59. Calvet, J.-C.; Wigneron, J.-P.; Walker, J.; Karbou, F.; Chanzy, A.; Albergel, C. Sensitivity of Passive Microwave Observations to Soil Moisture and Vegetation Water Content: L-Band to W-Band. *IEEE Trans. Geosci. Remote* **2011**, *49*, 1190–1199, doi:10.1109/TGRS.2010.2050488.